Medical Physics Letter

Full-field 3D photoacoustic imaging based on plane transducer array and spatial phase-controlled algorithm

Qiuzhen Zhou, Xuanrong Ji, and Da Xing[a)]
MOE Key Laboratory of Laser Life Science and Institute of Laser Life Science, College of Biophotonics, South China Normal University, Guangzhou 510631, China

(Received 6 October 2010; revised 22 December 2010; accepted for publication 25 January 2011; published 24 February 2011)

Purpose: Photoacoustic imaging (PAI) used for noninvasive imaging of biological tissue has been reported in many literature. However, there are still some disadvantages in the novel technique, such as the poor efficiency of imaging. In the current PAI, multiple excitation of laser and multiple acquisition of signal are necessary for image reconstruction. In this case, laser pulses may injure biological tissue due to energy accumulation. To popularize PAI in clinical applications, it is necessary to develop a new imaging approach to increase the efficiency of PAI.
Methods: A spatial phase-controlled algorithm is presented for full-field three-dimensional (3D) image reconstruction. By using the algorithm, photoabsorption sources at different depths can be reconstructed using just one set of data acquired in single laser shot. Unfocused plane transducer array and parallel data-acquisition (PDA) equipment are used for real-time photoacoustic (PA) signal detection and acquisition.
Results: The spatial resolution of the 3D PAI system was analyzed. Two graphite rods at various positions in a simulation model and two bifurcate vessels in the ear of rabbit were imaged. In addition, the motion trace of one particle flowing at constant velocity was captured dynamically. Experimental results showed that spatial phase-controlled algorithm based on plane transducer array and PDA system was capable of static and dynamic 3D PAI.
Conclusions: Spatial phase-controlled algorithm is introduced for 3D image reconstruction. The PA signals are collected by plane transducer array and PDA system in single pulse excitation. The acquired volumetric data are sufficient for 3D image reconstruction. Therefore, tissue can avoid the long-term exposure to light source and it is safer than the current PAI for *in vivo* imaging. With an increase in the repetition rate of laser pulse and speed of image display, the imaging method will realize real-time 3D imaging, which will be significant in clinical detection and medical diagnosis. © *2011 American Association of Physicists in Medicine*. [DOI: 10.1118/1.3555036]

Key words: PAI, spatial phase-controlled algorithm, plane transducer array, PDA, full-field 3D image reconstruction

I. INTRODUCTION

Photoacoustic imaging (PAI) is a novel noninvasive imaging modality based on the photoacoustic (PA) effect.[1–5] When laser pulse heats absorbing structures within biological tissue, ultrasonic wave that carried tissue optical absorption properties will be generated due to thermal expansion effect. PA detector collects signal in the process of ultrasonic propagation to map the distribution of radiation absorption with an image reconstruction algorithm.[3–8] PAI has been developed to be a promising medical imaging tool owing to its characteristic of combining the high tissue contrast of pure optical imaging and the high spatial resolution of pure ultrasonic imaging.[9–14]

However, current PAI faces challenges in clinical applications due to the poor efficiency of imaging. Signal collection system and capture mode are the two main factors the affect the efficiency of PAI. On one hand, although single-element transducer connected to digital oscilloscope is commonly used as an acquisition device as well as multielement linear transducer array combined with multichannel collecting system,[15,16,4,17,18] the gathering method of one-channel or electronic scanning based on time division multiplexing cannot satisfy the requirement of real-time data acquisition. Moreover, the detector needs to mechanically scan around PA objects or move near optical absorbers to obtain one clear reconstructed image, which may bring measurement errors to the reconstruction result due to the instability of signal acquisition system in the process of scanning.[19–22] On the other hand, single-element transducers and multielement linear transducer array are all plane-selective detectors. The collected data only come from the section where the detector is placed. Therefore, the detector has to be moved along different planes if three-dimensional (3D) image is necessary.[23,24] All the above reasons result in the poor efficiency of imaging. To our knowledge, a two-dimensional (2D) detector can

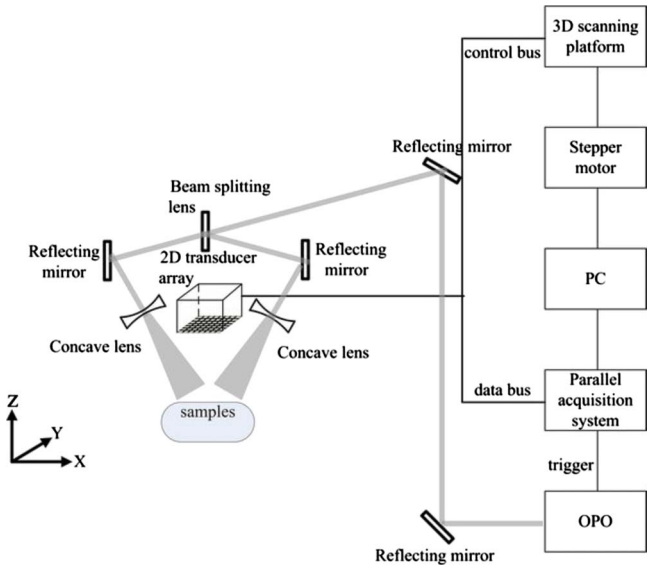

FIG. 1. Schematic diagram of the 3D PAI system; ultrasonic coupling medium is filled in between the plane transducer array and the samples.

map any optical absorber owning spatial morphology as long as it is placed in the detection range of the transducer. Therefore, 2D detector will be a desirable alternative to increase the efficiency of PAI.

In this work, we develop a new approach for real-time signal acquisition and full-field 3D image reconstruction. When optical absorbing structures are recorded by the plane transducer array and parallel data-acquisition (PDA) system without scanning detector or samples,[25,26] spatial phase-controlled algorithm is adopted to reconstruct the absorbing structures according to the spatial position of photoabsorption source and the weighting factor of the collected signal to every detector. The spatial resolution of the 3D PAI system was quantified. 3D images of two graphite rods and two bifurcate vessels in the ear of rabbit were obtained. In addition, the motion trace of one flowing particle was captured dynamically. The reconstruction results demonstrate that spatial phase-controlled algorithm based on the plane transducer array and PDA system is available for 3D PAI. It holds the potential for clinical detection and medical diagnosis.

II. IMAGING APPROACH

II.A. Setup

An imaging system has been developed for signal acquisition and image reconstruction. A schematic diagram of the system is shown in Fig. 1. An optical parametric oscillator (OPO) tunable laser (VIBRANT B 532I, OPOTEK, USA) is employed to produce 532 nm laser pulses (pulse width: 7 ns; repetition frequency: 10 Hz). A beam splitting lens divides the emitted laser pulse into two, with the same energy at an incident angle of 45°. Two concave lenses are adopted to enlarge irradiation region. (Two Gaussian beams overlap on a region with a diameter of 22 mm; the maximum energy of one pulse is limited to 19 mJ and the corresponding energy density is 5 mJ/cm^2, which complies to the ANSI safety standard.[27])

Plane transducer array is used to capture PA signals. The size of the transducer is $30\times30\times30$ mm (length, width, thickness, respectively.). 8×8 square piezoelectric detectors are distributed on the central area of the transducer (1 cm^2). The size of each element is 0.984 mm, that is, the same as the detector spacing. The main frequency and bandwidth are 7.5 MHz and 60%, respectively.

Compared to the one-channel or multichannel scanning acquisition system, the 64-channel PDA system is a great improvement for reducing data collecting time. It consist of a trigger acquisition module, an analog amplify circuit, an antialiasing filter module, analog-digital (A/D) conversion module, a data cache module, and a USB interface. Once trigger acquisition module is excited by the Q-switch signal of OPO, the 64-channel PDA system starts collecting. The raw PA signal is amplified by the analog amplify circuit (magnification is dynamically changed according to the distance between the PA source and the transducer, and the maximal gain is 40 dB) and filtered by the antialiasing filter module first. Subsequently, the pretreatment analog data are digitized by the analog-digital (A/D) conversion module. (The sampling rate is 40 Msamples/s and the sampling precision is 12-bit.) Finally, the digital volumetric data are stored into the data cache module and transmitted to a personal computer via USB interface.

One fixed device connected to a 3D scanning stage controls the plane transducer array to move arbitrarily, which is realized by stepper motor with LABVIEW control program. Therefore, any PA source at different position can be gathered. With PDA system, the detected signal can be acquired and transmitted every 1/100 s. Image reconstruction is completed in MATLAB (version 7.8, MathWorks, Natick, Massachusetts) and the run time of reconstruction algorithm is about 1 s. 3D visualization is fulfilled in 3D-Med (Institute of Automation, Chinese Academy of Sciences).

II.B. Spatial phase-controlled algorithm

In spatial phase-controlled algorithm, any detector should have recorded all light-absorbing objects in the detection area of the transducer according to spherical PA source theory. However, directivity pattern cannot be neglected because of the finite size of the detector;[28] only the PA signal confined in the maximal acceptance angle (decided by the size of the detector and the main frequency of the transducer) of array element can be measured in each acquisition.[29] Therefore, different optical absorbers in the same cross section can be simultaneously gathered by the corresponding element, and the optical absorbers at various depths will be resolved by measuring the time of arrival of PA pulses at each activated detector of the transducer and the ultrasonic velocity (time-resolved method). As shown in Fig. 2, P_m as the reconstruction pixel is calculated through following formula:

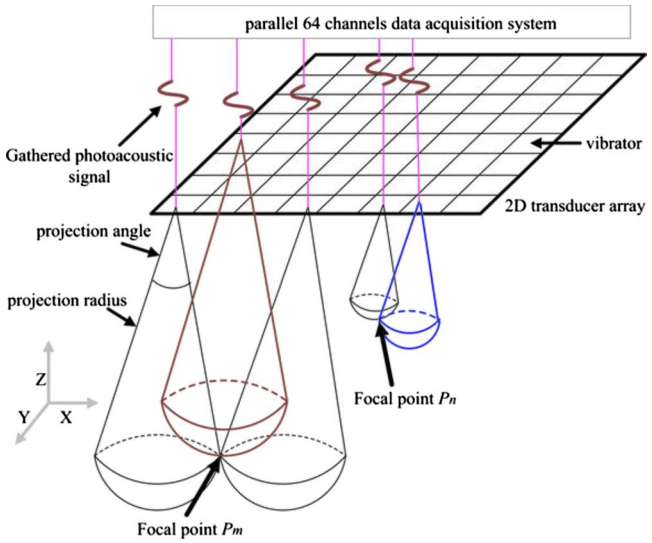

FIG. 2. Graphical illustration of the principle of imaging algorithm. Every detector will form some scan surfaces, so the PA source at any position can be deemed a dynamic focus.

$$P_m = \sum_{k=1}^{K} D(\theta)_k P(t_{mk}), \tag{1}$$

where m is the spatial vector of the PA source, k is the position of No. k detector, and K is the total number of working detectors. $D(\theta)$ is defined as the projection intensity weight function of θ (projection angle, which is no more than the maximal acceptance angle of the array element). $P(t_{mk})$ is the signal value collected by No. k detector at position m. $t_{mk} = r_{mk}/v$ represents the time when PA pulses spread from position m to k. r_{mk} is the distance between PA source at position m and No. k detector. v is the average velocity of the acoustic wave in the biological tissue. According to Eq. (1), the volumetric data collected by the plane transducer array in single laser pulse can be used to reconstruct 2D projection images at various depths. When different scanned surfaces overlap, the pixel of optical absorbers will become outstanding in reconstruction image. Therefore, spatial phase-controlled algorithm is practical for full-field 3D projection imaging.

III. RESULT

Spatial resolution of PA image is a key parameter for appraising the quality of the imaging approach. In the experiment of lateral resolution measurement, two black spherical cements with a diameter of 1 mm were imaged. The target specimen was embedded into a phantom at a depth of 1 mm. The distance between the detector surface and the 2D imaging section was about 3 cm. Figure 3(a) is the reconstructed image of the specimen corresponding to the photograph at the top right corner. Figure 3(b) is the normalization line profile of the reconstructed image shown in Fig. 3(a) at $x = 2.1$ cm. The profile includes two absorption sources. The 40.5% amplitude line intercepts with the profile at points A–D, respectively. The lateral resolution is estimated according to the Rayleigh criterion.[30,31] Therefore, the minimum distinguishable distance between the two sources is approximately R. $R = (|AB| + |CD|)/2 - 2r$, where r is the radius of the absorption source. R is measured to be about 1.8 mm. In the experiment of axial resolution measurement, two other specimens with a diameter of 1 mm were embedded into another phantom in the same way. The 2D imaging plane was perpendicular to the detector surface. The distances between the transducer and the two specimens are 2.75 and 3.25 cm, respectively. Figures 3(c) and 3(d) are the 2D PA reconstructed image and normalization line profile of Fig. 3(c) at $x = 2.1$ cm. Likewise, the axial resolution is calculated according to the Rayleigh criterion; the minimum distinguishable distance in the axial direction is about 0.5 mm.

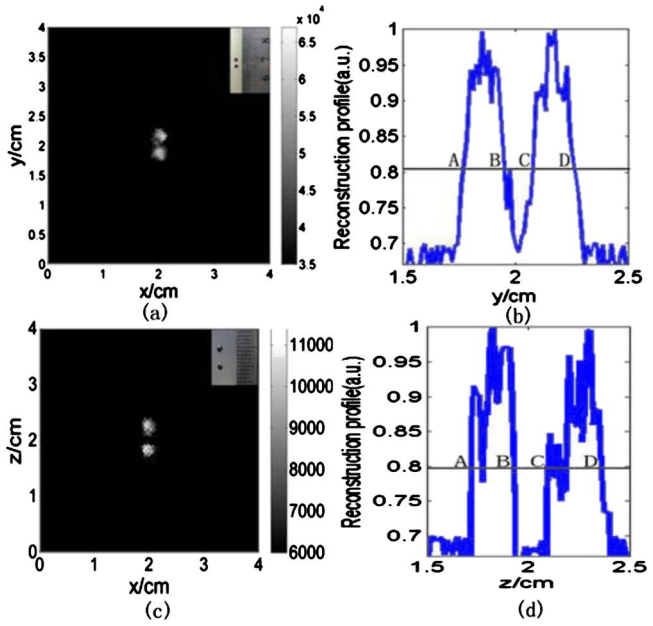

FIG. 3. Evaluating spatial resolutions. (a) Measuring lateral resolution. 2D lateral PA image of two black spherical cements corresponding to the photograph of the phantom; the center distance between the samples was about 5 mm. (b) Normalization line profile of the reconstruction image is shown in (a) with $x = 2.1$ cm. (c) Measuring axial resolution. 2D axial PA image of two black spherical cements corresponding to the photograph of the phantom; the center distance between the samples was about 5 mm. Z axis represents the distance between the sample and the plane transducer. (d) Normalization line profile of the reconstruction image is shown in (c) with $x = 2.1$ cm.

Three experiments were designed to verify the feasibility of the imaging method for full-field 3D PAI. In the simulation experiment, a cubic phantom made of 400 ml of water, 80 ml of milk (density: 0.8 g/ml), and 84 g of gelatin had been prepared. The phantom had an effective attenuation coefficient of 1.2 cm^{-1}, which agrees with the optical properties of human tissues.[10] Two graphite rods with a diameter of 0.5 mm were inserted into the phantom. One with a length of 7 mm is kept 45° with the upper side of the phantom. The other with a length of 3 mm was on a plane, which was apart from the detector with a distance of 3 cm. The detector above the samples and the phantom were all placed in a tank filled with ultrasonic coupling medium. Photographs of the phantom are exhibited in Fig. 4(a). Figure 4(b) is one frame 3D

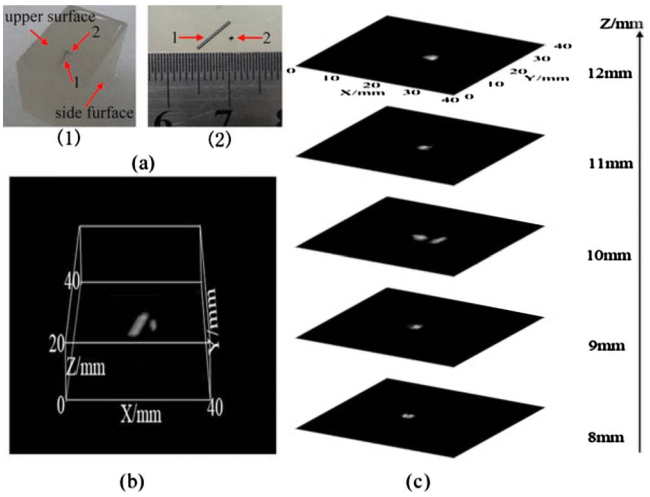

FIG. 4. (a) Photograph of the experimental sample. Two graphite rods with different lengths were embedded into a cubic phantom. The rod marked No. 1 was parallel to the side surface, keeping 45° with the upper surface. The rod marked No. 2 was parallel to the upper surface and perpendicular to the side surface. Transducer array was placed above the phantom and is parallel to the upper surface. Side picture of the sample was on the right, and the black point, represented as No. 2 rod, was perpendicular to the picture. (b) One frame 3D reconstructed PA image in a box of $40\times40\times20$ mm^3. To view the targets from different perspectives, an animation is offered in video 1 (video 1 available). (c) Five 2D full-field reconstruction slices corresponding to (b) in the *x*-*y* plane with an interval of 1 mm along the *Z* axis.

image shown in video 1, where the PA source at various depths is dynamically displayed, and selected 2D projection sections at different depths are shown in Fig. 4(c). It is obvious that the variation trend of target position in different slices shows the capability of the imaging way for static 3D imaging.

In the animal experiment, one New Zealand rabbit (5–6 kg) was selected for *in vivo* imaging. The solution of pentobarbital sodium (40 mg/kg) was used as anesthesia. Before PAI, the hair in the ear was removed with depilatory. To couple the PA signal, a window (40×40 mm^2) of polyethylene film at the bottom of the water tank was made. During the experiment, the rabbit lay under the tank and one of the ears was stick on the film. The imaged result of two bifurcate artery vessels is shown in Fig. 5. The 3D movie is offered in video 2.

In the dynamic experiment, a motion target at a velocity of 10 mm/s was captured dynamically. Silicone tube containing a particle (diameter: 1 mm) was set in the water tank, keeping a small angle with the detector surface. The particle was pushed forward by water flow, which could be realized through standard syringe connected to an infusion pump. The data-collection interval was 0.1 s due to the restriction of repetition rate of the laser pulse. The object position in each PA excitation was captured successfully. Figure 6 exhibits one position of the motion particle. Motion trace of the object is displayed offline in video 3. The result proves that dynamic detection of motion object can be realized by the imaging approach.

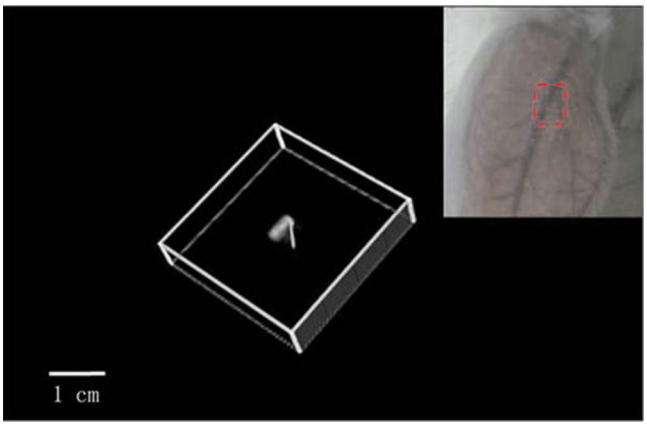

FIG. 5. 3D image of two bifurcate artery vessels. The inset picture is the photo of rabbit's ear; the dashed rectangle indicates the imaged region. The diameters of these two vessels are about 1.5 and 0.6 mm, respectively. The 3D movie is offered in video 2 (video 2 available).

IV. DISCUSSION AND CONCLUSION

Full-field 3D imaging can be accomplished with the spatial phase-controlled algorithm based on the plane detector and PDA system, despite the lateral resolution of PA image is not very well. As we know, spatial resolution is influenced by the number of transducer elements, the interval of elements, and the bandwidth. The number of transducer elements and interval of elements are the two most important factors deciding the lateral resolution. Increasing the number of elements and reducing the interval of elements can improve the lateral resolution. Potentially, the optimal lateral resolution may reach the limiting lateral resolution, which is decided by the interval of unfocused detector elements. Axial resolution depends on the main frequency and bandwidth. Therefore, developing broad bandwidth and high integration density 2D transducer array will be an effective approach to improve the spatial resolution of reconstruction image. In addition, PA signal is captured just in single laser shot. Therefore, the collected PA signal is weaker compared to the signal captured in multiple excitation. If the sensitivity of the detector can improved, the signal to noise ratio will be increased, which is also useful for improving the spatial resolution of the image.

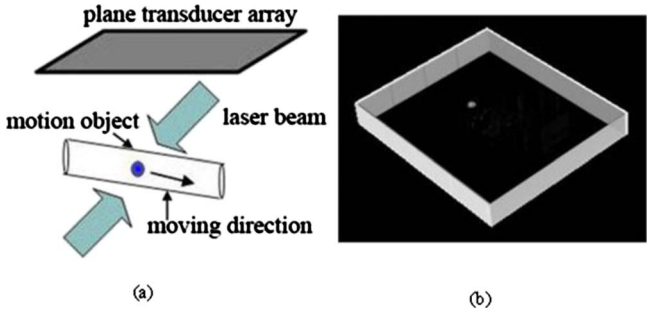

FIG. 6. (a) Schematic diagram of the experimental models. (b) One frame image in video 3 of PAI of one motion object (video 3 available).

3D PAI with a variety of approaches has been discussed in many literature. These can be classified as scanning method and nonscanning method. No matter single-detector-based photoacoustic microscope or acquisition system based on linear detector,[32–38] transducer needs to move along the detection surface for 3D image collection. Therefore, several hours may be spent even if the spatial resolution of reconstruction image is satisfactory ($\sim\mu$m) and it is infeasible in clinical diagnosis.

2D staring array of transducer used for ultrasound detection is an effective solution to increase the efficiency of imaging. Fast 3D PAI based on curved sparse array has been presented by Ephrat *et al.*[39,40] Compared to the array of curved geometry, the coverage of plane transducer array is less uniform in three coordinate directions, which results in nonisotropic spatial resolution (axial resolution is better than lateral resolution). However, the number of sparse array is few to obtain PA image with a better resolution. In addition, the spatial resolution of 3D image is different at various positions due to the limited acceptance angle of the detector. The optical absorber located at the crossing point of the axis of detector should be mapped with better contrast and resolution relative to other targets. Nevertheless, plane transducer array can image the absorption sources more homogeneously. For *in vivo* determination, the plane transducer array is more convenient and universal. However, the sparse array of curved geometry is only suitable for some special biological tissue (e.g., brain and breast).

In conclusion, spatial phase-controlled algorithm based on plane transducer array and PDA system has been used for full-field 3D PAI. Any optical absorber placed in the detection region of detector can be recorded and reconstructed fast. The detector need not to scan for multidirectional 2D projection imaging or move along different planes for 3D imaging. Furthermore, only one set of collected data in single pulse excitation is adequate for full-field 3D image reconstruction. Therefore, biological tissue can avoid the long-term exposure to light source. The result of animal experiment proves that the novel imaging approach will be safer than traditional PAI for *vivo* imaging. The motion trace of moving target has been dynamically monitored through our experiment. Therefore, if the repetition rate of laser pulse and the speed of image display can be increased in the future, the imaging method will have great potential for providing real-time 3D PAI without inflicting any harm to biological tissue, which will be significant in clinical detection and medical diagnosis. In addition, it will be an interesting direction to take advantage of the approach for dynamic monitoring of the variation of the exotic body in some blood disease diagnosis researches.

ACKNOWLEDGMENTS

This research was supported by the National Basic Research Program of China (Grant Nos. 2010CB732602 and 2011CB910402), the Program for Changjiang Scholars and Innovative Research Team in University (Grant No. IRT0829), and the National Natural Science Foundation of China (Grant No. 30870676).

[a]Electronic mail: xingda@scnu.edu.cn

[1]E. Zhang, J. Laufer, and P. Beard, "Backward-mode multiwavelength photoacoustic scanner using a planar Fabry-Perot polymer film ultrasound sensor for high-resolution three-dimensional imaging of biological tissues," Appl. Opt. **47**(4), 561–577 (2008).
[2]C. H. Li, A. Aguirre, J. Gamelin, A. Maurudis, Q. Zhu, and L. V. Wang, "Real-time photoacoustic tomography of cortical hemodynamics in small animals," J. Biomed. Opt. **15**(1), 010509 (2010).
[3]X. D. Wang, Y. J. Pang, G. Ku, X. Y. Xie, G. Stoica, and L. V. Wang, "Noninvasive laser-induced photoacoustic tomography for structural and functional in vivo imaging of the brain," Nat. Biotechnol. **21**(7), 803–806 (2003); D. W. Yang, D. Xing, H. M. Gu, Y. Tan, and L. M. Zeng, "Fast multielement phase-controlled photoacoustic imaging based on limited-field-filtered back-projection algorithm," Appl. Phys. Lett. **87**(19), 194101 (2005).
[4]L. M. Zeng, D. Xing, H. M. Gu, D. W. Yang, S. H. Yang, and L. Z. Xiang, "High antinoise photoacoustic tomography based on a modified filtered backprojection algorithm with combination wavelet," Med. Phys. **34**(2), 556–563 (2007).
[5]R. J. Zemp, R. Bitton, M. L. Li, K. K. Shung, G. Stoica, and L. V. Wang, "Photoacoustic imaging of the microvasculature with a high-frequency ultrasound array transducer," J. Biomed. Opt. **12**(1), 010501 (2007); Z. Yuan and H. B. Jiang, "Three-dimensional finite-element-based photoacoustic tomography: Reconstruction algorithm and simulations," Med. Phys. **34**(2), 538–546 (2007).
[6]L. V. Wang, "Prospects of photoacoustic tomography," Med. Phys. **35**(12), 5758–5767 (2008).
[7]C. G. A. Hoelen, F. F. M. deMul, R. Pongers, and A. Dekker, "Three-dimensional photoacoustic imaging of blood vessels in tissue," Opt. Lett. **23**(8), 648–650 (1998).
[8]X. D. Wang, Y. J. Pang, G. Ku, G. Stoica, and L. V. Wang, "Three-dimensional laser-induced photoacoustic tomography of mouse brain with the skin and skull intact," Opt. Lett. **28**(19), 1739–1741 (2003).
[9]M. Roumeliotis, P. Ephrat, J. Patrick, and J. J. L. Carson, "Development and characterization of an omni-directional photoacoustic point source for calibration of a staring 3D photoacoustic imaging system," Opt. Express **17**(17), 15228–15238 (2009).
[10]Y. Wang, D. Xing, Y. G. Zeng, and Q. Chen, "Photoacoustic imaging with deconvolution algorithm," Phys. Med. Biol. **49**(14), 3117–3124 (2004).
[11]S. Manohar, S. E. Vaartjes, J. C. G. Hespen, J. M. Klaase, F. M. Engh, W. Steenbergen, and T. G. Leeuwen, "Initial results of in vivo non-invasive cancer imaging in the human breast using near-infrared photoacoustics," Opt. Express **15**(19), 12277–12285 (2007).
[12]X. D. Wang, G. Ku, M. A. Wegiel, D. J. Bornhop, G. Stoica, and L. V. Wang, "Noninvasive photoacoustic angiography of animal brains in vivo with near-infrared light and an optical contrast agent," Opt. Lett. **29**(7), 730–732 (2004).
[13]G. Ku, X. D. Wang, X. Y. Xie, G. Stoica, and L. V. Wang, "Imaging of tumor angiogenesis in rat brains in vivo by photoacoustic tomography," Appl. Opt. **44**(5), 770–775 (2005).
[14]M. Eghtedari, A. Oraevsky, J. A. Copland, N. A. Kotov, A. Conjusteau, and M. Motamedi, "High sensitivity of in vivo detection of gold nanorods using a laser optoacoustic imaging system," Nano Lett. **7**(7), 1914–1918 (2007).
[15]H. Guo and S. H. Yang, "Photoacoustic tomography imaging system based on digital B-mode ultrasound diagnosis equipment," Rev. Sci. Instrum. **80**(11), 014903 (2009).
[16]K. H. Song and L. V. Wang, "Noninvasive photoacoustic imaging of the thoracic cavity and the kidney in small and large animals," Med. Phys. **35**(10), 4524–4529 (2008).
[17]B. Z. Yin, D. Xing, Y. Wang, Y. G. Zeng, Y. Tan, and Q. Chen, "Fast photoacoustic imaging system based on 320-element linear transducer array," Phys. Med. Biol. **49**(7), 1339–1346 (2004).
[18]L. M. Nie, D. Xing, D. W. Yang, L. M. Zeng, and Q. Zhou, "Detection of foreign body using fast thermoacoustic tomography with a multielement linear transducer array," Appl. Phys. Lett. **90**(17), 174109 (2007).
[19]G. Paltauf, R. Nuster, and P. Burgholzer, "Weight factors for limited angle photoacoustic tomography," Phys. Med. Biol. **54**(11), 3303–3314 (2009).
[20]S. Hu, K. Maslov, and L. V. Wang, "Noninvasive label-free imaging of

microhemodynamics by optical-resolution photoacoustic microscopy," Opt. Express **17**(9), 7688–7693 (2009).
[21]D. W. Yang, D. Xing, Y. Tan, H. M. Gu, and S. H. Yang, "Integrative prototype B-scan photoacoustic tomography system based on a novel hybridized scanning head," Appl. Phys. Lett. **88**(17), 174101 (2006).
[22]D. W. Yang, D. Xing, S. H. Yang, and L. Z. Xiang, "Fast full-view photoacoustic imaging by combined scanning with a linear transducer array," Opt. Express **15**(23), 15566–15575 (2007).
[23]L. Song, C. H. Kim, K. Maslov, and L. V. Wang, "High-speed dynamic 3D photoacoustic imaging of sentinel lymph node in a murine model using an ultrasound array," Med. Phys. **36**(8), 3724–3729 (2009).
[24]H. F. Zhang, K. Maslov, M. L. Li, G. Stoica, and L. V. Wang, "In vivo volumetric imaging of subcutaneous microvasculature by photoacoustic microscopy," Opt. Express **14**(20), 9317–9323 (2006).
[25]S. Manohar, A. Kharine, J. Hespen, W. Steenbergen, and T. Leeuwen, "The Twente photoacoustic mammoscope: System overview and performance," Phys. Med. Biol. **50**(11), 2543–2557 (2005).
[26]O. Balogun, B. Regez, H. F. Zhang, and S. Krishnaswamy, "Real-time full-field photoacoustic imaging using an ultrasonic camera," J. Biomed. Opt. **15**(2), 021318 (2010).
[27]American National Standards Institute, *American National Standard for the Safe Use of Lasers in Health Care facilities: Standard Z136.1-2000* (ANSI, Inc., New York, 2000).
[28]V. Kozhushko, T. Khokhlova, A. Zharinov, I. Pelivanov, V. Solomatin, and A. Karabutov, "Focused array transducer for two-dimensional optoacoustic tomography," J. Acoust. Soc. Am. **116**(3), 1498–1506 (2004).
[29]C. H. Li, G. Ku, and L. V. Wang, "Negative lens concept for photoacoustic tomography," Phys. Rev. E **78**(2), 021901 (2008).
[30]L. M. Nie, D. Xing, Q. Zhou, D. W. Yang, and H. Guo, "Microwave-induced thermoacoustic scanning CT for high-contrast and noninvasive breast cancer imaging," Med. Phys. **35**(9), 4026–4032 (2008).
[31]S. H. Yang, D. Xing, Q. Zhou, L. Z. Xiang, and Y. Q. Lao, "Functional imaging of cerebrovascular activities in small animals using high-resolution photoacoustic tomography," Med. Phys. **34**(8), 3294–3301 (2007).
[32]S. Hu, K. Maslov, and L. V. Wang, "In vivo functional chronic imaging of a small animal model using optical-resolution photoacoustic microscopy," Med. Phys. **36**(6), 2320–2323 (2009).
[33]J. Gamelin, A. Aguirre, A. Maurudis, F. Huang, D. Castillo, L. V. Wang, and Q. Zhu, "Curved array photoacoustic tomographic system for small animal imaging," J. Biomed. Opt. **13**(2), 024007 (2008).
[34]X. D. Wang, Y. Xu, M. H. Xu, S. Yokoo, E. S. Fry, and L. V. Wang, "Photoacoustic tomography of biological tissues with high cross-section resolution: Reconstruction and experiment," Med. Phys. **29**(12), 2799–2805 (2002).
[35]L. Song, K. Maslov, K. K. Shung, and L. V. Wang, "Ultrasound-array-based real-time photoacoustic microscopy of human pulsatile dynamics in vivo," J. Biomed. Opt. **15**(2), 021303 (2010).
[36]L. Song, K. Maslov, R. Bitton, K. K. Shung, and L. V. Wang, "Fast 3-D dark-field reflection-mode photoacoustic microscopy in vivo with a 30-MHz ultrasound linear array," J. Biomed. Opt. **13**(5), 054028 (2008).
[37]L. Song, K. Maslov, and L. V. Wang, "Section-illumination photoacoustic microscopy for dynamic 3D imaging of microcirculation in vivo," Opt. Lett. **35**(9), 1482–1484 (2010).
[38]R. J. Zemp, L. Song, R. Bitton, K. K. Shung, and L. V. Wang, "Realtime photoacoustic microscopy in vivo with a 30-MHz ultrasound array transducer," Opt. Express **16**(11), 7915–7928 (2008).
[39]P. Ephrat, M. Roumeliotis, F. S. Prato, and J. J. Carson, "Four-dimensional photoacoustic imaging of moving targets," Opt. Express **16**(26), 21570–21581 (2008).
[40]P. Ephrat, L. Keenliside, A. Seabrook, F. S. Prato, and J. J. L. Carson, "Three-dimensional photoacoustic imaging by sparse-array detection and iterative image reconstruction," J. Biomed. Opt. **13**(5), 054052 (2008).